Chapter 8
Mantle-Derived Carbonate Fluid Alteration and Gold Mineralization in Southern Granulite Terrain, Wynad, India

K.L. Pruseth, V. Ravikant, S. Varghese, and R. Krishnamurthi

Introduction

Large-scale carbonate deposition and replacement in shear zones from various terrains, that are part of regional carbonate alteration, usually host significant gold mineralization (e.g. Kerrich, 1990; Kerrich et al., 1987; Groves et al., 1989; Barnicoat et al., 1991; Goldfarb et al., 2001; Groves et al., 2003). Though the carbonate permeations are generally perceived as evidence for localized, high CO_2 fluxes into the crust, the source(s) of these fluids is controversial. Evidence for regional carbonate alteration of the crust by fluids from mantle-derived magmas (alkalic basalt, syenite and carbonatite) was presented for the Attur shear zone of Tamil Nadu (Fig. 8.1a, map from Santosh and Sajeev, 2006) by Wickham et al. (1994). We relate the occurrences of the auriferous veins of Wynad (Fig. 8.1b) (Binu Lal et al., 2003) to similar carbonate alteration zones, along the regional Moyar shear zone, where gold-hosted quartz-pyrite hydrothermal veins are well known, but the source rocks for the gold remains unclear.

Here, unlike the Archaean greenstone-hosted gold deposits normally found in India, we report newly identified quartz-carbonate (both ferroan calcite and ankerite) dykes of Wynad that have a direct continuity with the auriferous quartz veins. Distinct mantle value of initial Sr isotopic composition from these dykes, strongly suggests that this orogenic gold was carried and precipitated by mantle-derived carbonate-rich hydrothermal fluids. This mantle component probably was initiated due to structural and thermal events, synchronous with or post-dating orogeny (Goldfarb et al., 2001), specifically the Pan-African orogeny along the Moyar shear zone.

————————————————

K.L. Pruseth (✉)
Department of Geology & Geophysics, Indian Institute of Technology, Kharagpur-721302, India
e-mail: klpruseth@gmail.com

V. Ravikant
Indian Institute of Science Education and Research-Kolkata, Mohanpur 721452, India

S. Varghese and R. Krishnamurthi
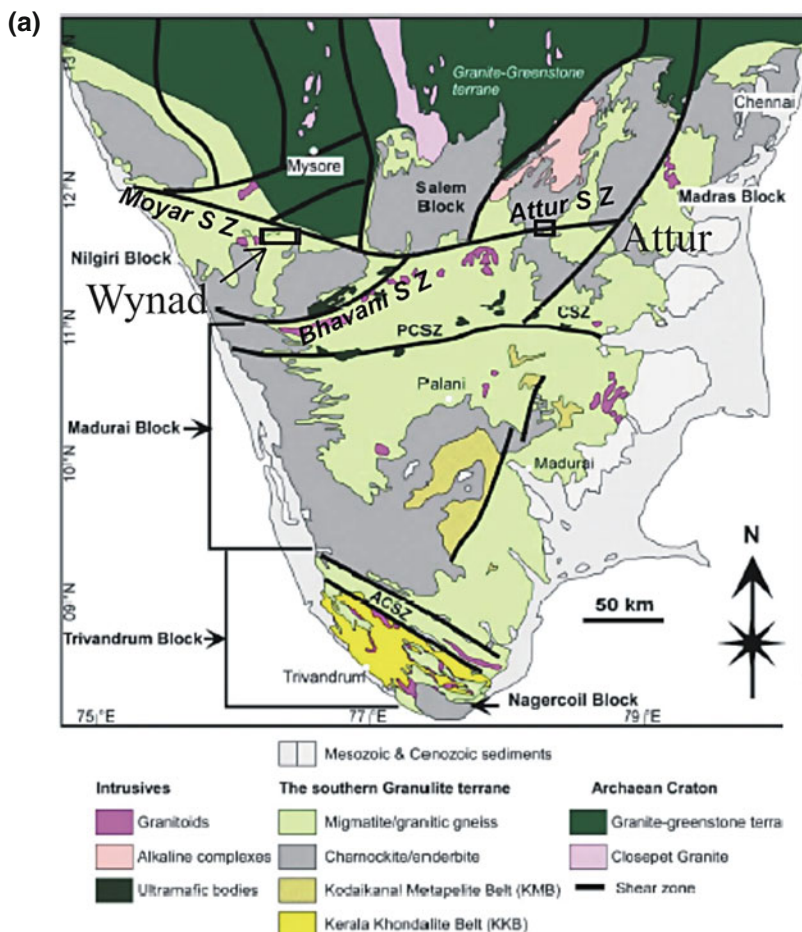Department of Earth Sciences, Indian Institute of Technology, Roorkee 247667, India

Fig. 8.1 (**a**) Geological map of the Southern Granulite Terrain (from Santosh and Sajeev, 2006) showing location of the Wynad gold field, south of the Moyar shear zone; location of the Attur shear zone, Tamil Nadu is also shown. (**b**) Sketch geological map of the Wynad gold field (after Binu Lal et al., 2003)

Geologic Setting

The Wynad Gold Field (WGF) occurs within the northernmost part of the Southern Granulite Terrain, north of the ∼2.5 Ga enderbitic Nilgiri massif and immediately south of the Moyar shear zone (Fig. 8.1a). The WGF comprises a network of auriferous hydrothermal quartz veins (individual veins of length >100 m, average thickness of ∼1.5 m) within Precambrian migmatitic tonalitic gneisses and granulites (Nair and Suresh, 1994; Binu Lal et al., 2003., Malathi and Srikantappa, 2005). Whereas the enderbitic remnants are part of the Late Archaean Nilgiri
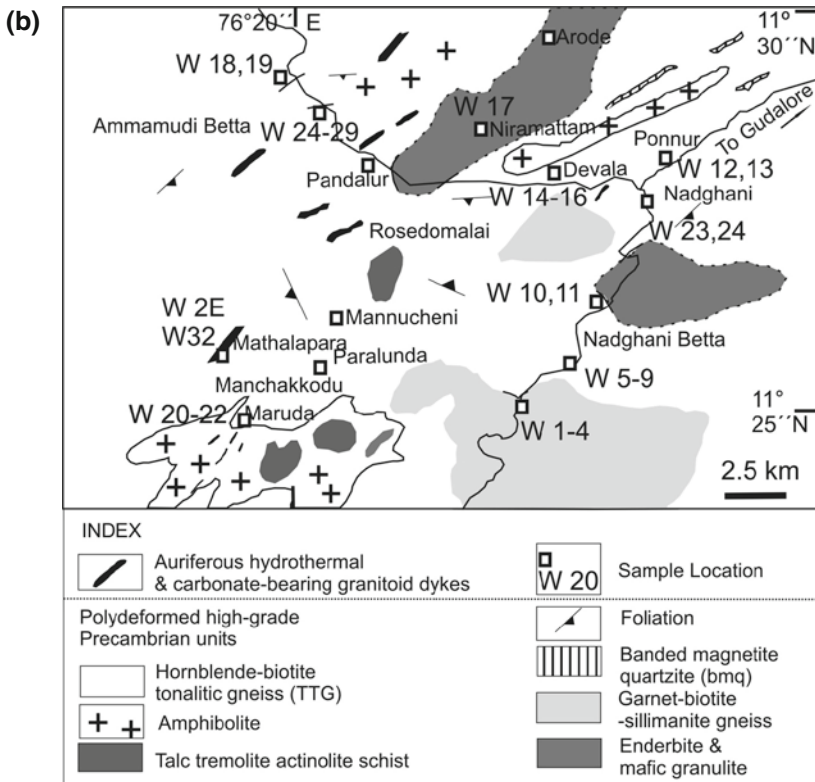
Fig. 8.1 (continued)

granulites (Ghosh et al., 2004), lenticular banded magnetite-quartzite, amphibolite (retrogressed mafic granulite) and minor charnockite are interbanded with the polydeformed migmatitic tonalitic gneisses; a few late, undeformed intrusives of pegmatites have been observed.

Gold-bearing quartz veins, with minor pyrite, muscovite and calcite, form a network that cross-cuts amphibolite and hornblende-biotite quartzo-feldspathic (tonalitic) gneisses to the south and southwest of Wynad (around Maruda, Devala and Pandalur, shown on Fig. 8.1b). Furthermore, these high-grade metamorphic, polydeformed rocks are intruded by unusual pinkish to grey quartz-carbonate dykes and pods, and the auriferous veins can be clearly traced to these dykes (Fig. 8.2a, b).

The most important observation is that there appear to be stages in the hydrothermal evolution of these quartz veins and from field evidence they are seen to emanate from distinct, hitherto unrecognized, quartz-carbonate dykes and pods. These stages recording different mineral assemblages from source rock to barren milky white quartz veins are given below according to their probable sequence of formation:
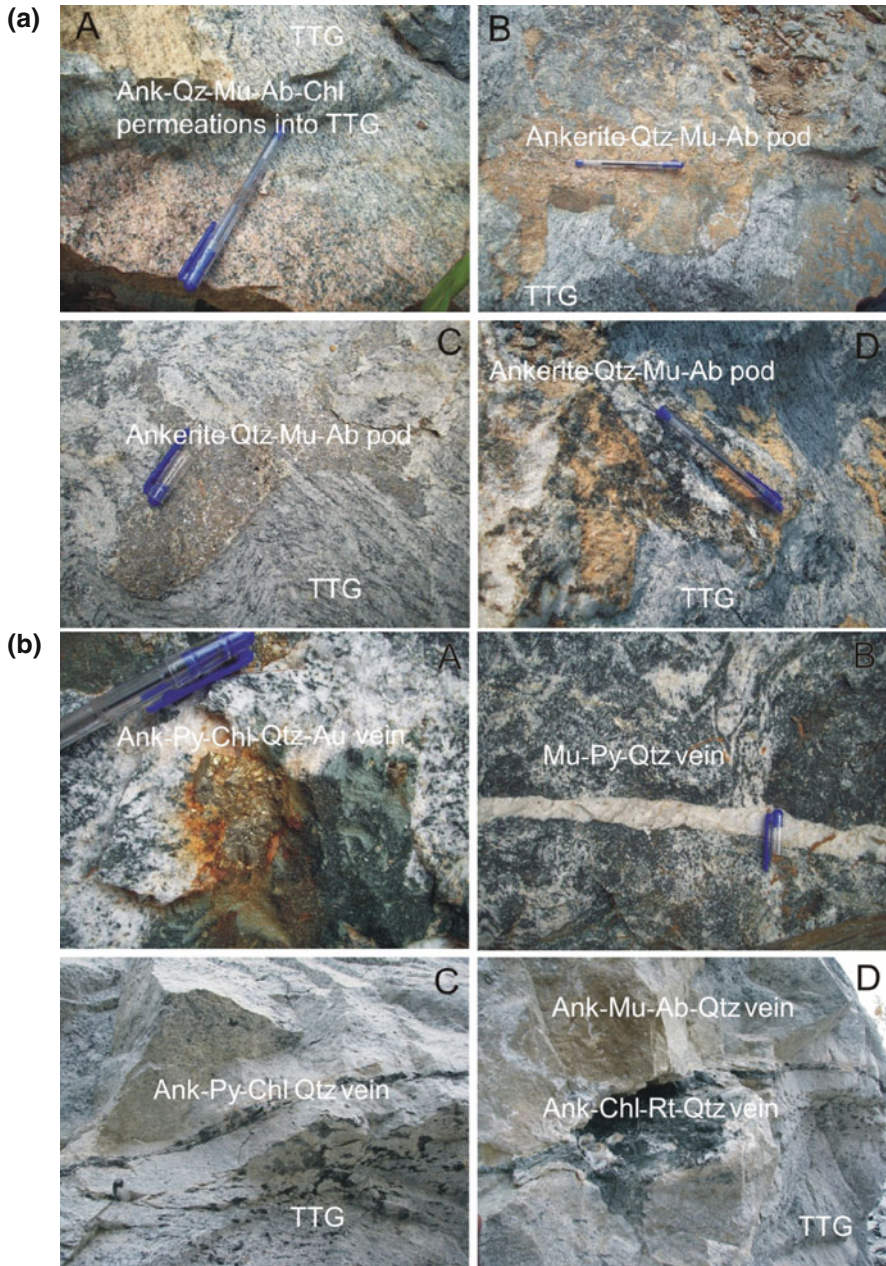
Fig. 8.2 (**a**) A to D. Field relations of the quartz-carbonate muscovite, albite, chlorite dykes intruding the tonalitic gneisses (TTG) from around Pandalur and Maruda, Wynad (carbonate alteration). (**b**) A to D. Field relations of auriferous hydrothermal veins clearly showing emplacement along dilatant and brittle fractures as observed around Maruda

Quartz-carbonate dykes: quartz + pyrite ± pyrrhotite + muscovite + albite + chlorite + carbonate + hematite ± gold ± zircon (Fig. 8.2a, A & D)

Quartz-carbonate dykes (sub-volcanic textured): with megacrysts of muscovite and ankerite and ferroan calcite (Fig. 8.2a, B & C)

Hydrothermal vein (primary auriferous quartz veins): quartz + pyrite ± pyrrhotite + chalcopyrite + gold + muscovite ± chlorite ± carbonate (Fig. 8.2b, A, B & C)

Hydrothermal vein: secondary veins with vugs that contain quartz, chlorite, rutile and scalenohedral pink calcite (Fig. 8.2b, D)

Milky white quartz veins: with traces of muscovite.

Analytical Methods

Pyrite separated from chips of the Wynad hydrothermal veins were washed in deionized water, dried and crushed manually to coarse grains in an agate mortar. Clean crystals of pure pyrite were hand picked from this crushed mixture immersed in ethanol and dried. Water-soluble components of fluid inclusions were released by powdering the sulfides in an agate mortar in ∼5–10 ml of ultrapure water (crush-leach method). Similar methods have been successfully used by Bottrell et al. (1988), Banks et al. (1992), Christensen et al. (1995) and Channer et al. (1999). The fluid was rinsed off twice through a grade 292 Sartorius filter paper and collected; fine mineral powder was collected from the dried filter paper.

Trace elements were analyzed on a Perkin-Elmer Sciex ELAN DRC-e ICP-MS at the Institute Instrumentation Centre, IIT, Roorkee (following Ravikant, 2010). About 30 mg of the pyrite fluid and residue, and powdered samples of seven white calcites was digested in Savillex vials using conc. $HCl + HNO_3$ (3:1) mixture followed by conc. HCl, and diluted to 100 ml in ultrapure 2% HNO_3. Ten ppb of Rh and In were added as internal standards. The dried fluid leachate was dissolved in 10 ml ultrapure water and used for analysis. Basalt rock reference standards United States Geological Survey (USGS) BCR 2 and Geological Survey of Japan (GSJ) JB 2 were used to externally calibrate element concentrations. Analytical precisions were <6% for HFSE and transitional elements, <2% for Ba, Sr and Rb, <5% for LREE and <7% for MREE and HREE. Trace element concentrations of selected samples are given in Tables 8.1 and 8.2.

For Rb-Sr geochronology, the USGS and GSJ rock reference samples AGV 2, BCR 2, W 2 and JB 2, JGb 1 and JA2, respectively, were used to check the accuracy of the procedure. Whole rock, muscovite separates, carbonate (calcite) from the quartz-carbonate dykes and pyrite residues from the auriferous hydrothermal veins were digested using conventional conc. $HF + HNO_3$ and conc. HCl and conc. $HNO_3 + HCl$ method, respectively. Rubidium and Sr from all samples and fluid leachates were separated using conventional cation exchange chromatography, on primary quartz glass columns packed with 4 ml BioRad resin AG 50×50 200–400 mesh, using 2N HCl as eluent. Strontium (in 1 M HNO_3) and Rb (in MilliQ water) were loaded on degassed single W filaments with 1 µl TaF_5 activator.

Table 8.1 Trace element concentrations (in μg/g) and diagnostic ratios in selected fluids from Wynad pyrite (pyfl), chondrite normalizing values of McDonough et al. (1991)

Element	W21 Cpyfl	W21 Dpyfl	W21 Epyfl	W22 ACpyfl	W22 BCpyfl	W23 ACpyfl	W23 Bpyfl	W24 Apyfl	W26 Apyfl	W27 Apyfl	W27 Bpyfl	W28 Apyfl	W28 Bpyfl
Co	28	219	70	31	8.5	14	12	5.5	3.3	5.7	2.5	0.92	0.40
Cr	6.5	7.2	7.9	8.4	7.6	7.5	6.9	9.9	3.3	6.9	5.5	6.4	4.2
Ni	77	139	72	105	44	38	47	96	5.0	20	32	9.4	3.9
Rb	287	341	361	348	189	263	127	38	16	100	75	41	15
Ba	16	23	13	12	8.4	6.3	7.8	7.5	1.5	5.8	4.3	3.1	1.0
Th	0.9	0.4	0.6	0.4	0.8	0.6	1.2	0.2	0.1	0.7	0.8	0.9	0.9
U	84	130	106	97	103	69	89	62	30	47	42	45	13
Nb	0.31	0.22	0.25	0.22	0.31	0.22	0.13	0.14	0	0.13	0.11	0.13	0
Ta	3.2	3.6	3.9	1.5	4	1.2	1.7	0.56	0	0.93	0.32	0.7	0.8
Sr	87	130	71	71	60	29	58	48	1.7	25	22	17	3.0
Hf	0.13	0.14	3	0.13	0.1	0.03	0.03	0.02	0.01	0.01	0.03	0.03	0.04
Zr	0.13	0.14	0.15	0.13	0.14	0.11	0.15	0.03	0.02	0.16	0.12	0.11	0.04
Y	0.32	2.9	0.34	0.25	0.37	0.36	0.14	0.17	0.12	0.22	0.15	0.24	0.14
La	2.3	32	3.1	1.8	2.3	2.1	1.3	0.54	1.3	1.4	1.3	1.5	1.4
Ce	1.6	14	2.0	1.2	1.7	1.5	0.91	0.32	0.85	1.0	1.0	1.2	1.0
Pr	1.3	10	2.0	1.1	1.6	1.4	0.8	0.33	0.65	0.92	0.91	1.1	0.83
Nd	1.1	8.1	1.4	0.96	1.4	1.4	0.77	0.26	0.48	0.75	0.70	0.85	0.67
Sm	1.2	4.6	1.3	1.0	1.2	1.0	0.59	0.38	0.33	0.66	0.59	0.56	0.45

Table 8.1 (continued)

Element	W21 Cpyfl	W21 Dpyfl	W21 Epyfl	W22 ACpyfl	W22 BCpyfl	W23 ACpyfl	W23 Bpyfl	W24 Apyfl	W26 Apyfl	W27 Apyfl	W27 Bpyfl	W28 Apyfl	W28 Bpyfl
Eu	1.4	2.7	1.0	0.91	0.81	0.87	0.80	0.43	0.35	0.60	0.48	0.73	0.37
Gd	1.0	3.6	0.92	0.68	0.77	0.74	0.57	0.26	0.30	0.48	0.46	0.65	0.34
Tb	0.62	4.5	0.83	0.46	0.72	0.60	0.33	0.10	0.25	0.36	0.44	0.58	0.31
Dy	0.57	3.9	0.56	0.40	0.58	0.50	0.27	0.13	0.23	0.36	0.37	0.42	0.28
Ho	0.64	4.42	0.63	0.52	0.60	0.70	0.29	0.13	0.16	0.38	0.35	0.47	0.33
Er	0.65	4.0	0.53	0.45	0.52	0.63	0.24	0.11	0.19	0.28	0.34	0.44	0.22
Tm	0.71	3.30	0.60	0.50	0.59	0.70	0.32	0.14	0.18	0.34	0.32	0.42	0.30
Yb	1.0	4.3	0.85	0.83	0.96	1.1	0.44	0.21	0.35	0.64	0.63	0.78	0.41
Lu	0.71	2.57	0.60	0.50	0.59	0.70	0.32	0.14	0.18	0.34	0.32	0.42	0.30
Σ REE	15	102	16	11.3	14.4	14	7.9	3.3	5.7	8.4	8.2	10.1	7.1
$(La/Sm)_{CN}$	1.9	6.9	2.5	1.7	1.9	2.0	2.2	1.2	3.8	2.1	2.2	2.7	3.0
$(La/Yb)_{CN}$	2.1	7.5	3.7	2.1	2.4	1.8	3.0	2.3	3.5	2.2	2.0	1.9	3.3
$(Dy/Yb)_{CN}$	0.53	0.92	0.66	0.48	0.60	0.44	0.62	0.60	0.65	0.56	0.58	0.53	0.69

Table 8.2 Trace element concentrations (in μg/g) and diagnostic ratios in selected calcite from auriferous hydrothermal veins of Wyand, chondrite normalizing values of McDonough et al. (1991)

Element	W32B cc	W32C cc	W32F cc	W32G cc	W32H cc	W32I cc	W32J cc
Co	15	11	15	4.7	1.8	6.9	4.9
Cr	1.4	2.3	1.6	2.1	1.4	1.7	1.9
Sc	13	5.5	17	3.4	0	5.4	5.5
Ni	4.5	3.1	2.5	1.9	2.5	2.7	3.2
Rb	1.5	2.4	1.9	6.1	3.6	2.1	2.4
Ba	5	6.3	5.6	18	5.6	7.9	4.2
Th	0.80	0.25	0.23	0.22	0.13	0.21	0.22
U	0.27	0.06	0.10	0.10	0.05	0.04	0.05
Nb	3.8	1.9	1.8	2.2	1.9	1.3	2.0
Ta	16	5.2	6	7.2	4.5	5.2	7.1
Sr	8,165	6,162	8,547	5,522	6,469	7,389	7,230
Hf	4.1	2.1	4.2	4.7	1.1	0.96	0.78
Zr	65	26	48	58	14	7.7	8.7
Y	1,268	684	1,489	150	156	638	519
La	41	13	37	18	8.9	17	20
Ce	24	9.2	24	11	5.9	11	13
Pr	20	7.7	21	9.3	4.9	9.3	11
Nd	16	6.6	18	7.4	3.9	7.8	8.8
Sm	12	5.2	15	4.0	2.6	6.0	6.1
Eu	41	11	32	5.8	6.3	14	14
Gd	29	9.7	27	4.4	4.4	11	11
Tb	16	7.8	21	3.0	2.5	8.0	7.2
Dy	16	8.1	21	2.6	2.4	8.6	6.5
Ho	17	9.2	21	2.5	2.4	9.1	6.9
Er	15	8.3	18	2.3	2.2	8.6	6.0
Tm	16	9.5	20	2.3	2.2	8.9	6.5
Yb	25	14	31	3.3	3.7	15	10
Lu	14	7.7	17	1.7	1.9	7.8	5.8
Σ REE	303	128	323	78	55	142	1,323
(La/Sm)$_{CN}$	3.4	2.5	2.4	4.4	3.4	2.8	3.2
(La/Yb)$_{CN}$	1.6	0.95	1.2	5.4	2.4	1.1	1.9
(Dy/Yb)$_{CN}$	0.61	0.58	0.67	0.77	0.65	0.58	0.63

Isotopic analyses of Rb and Sr were carried out on a Thermo Finnigan Triton T1 thermal ionization mass spectrometer, in static multicollector mode, at the National Facility for Geochronology and Isotope Geology at the Indian Institute of Technology, Roorkee. Mass fractionation corrections in Sr isotopic analyses were done with $^{86}Sr/^{88}Sr = 0.1194$. The precision of $^{87}Sr/^{86}Sr$ (0.03%) ratios are the external precisions based on replicate determinations of standards; precision on the $^{87}Rb/^{86}Sr$ ratio is 1% by IDTIMS. During the period of this study, the mean $^{87}Sr/^{86}Sr$ ratio was 0.71026 ± 0.00008 (2σ, $n = 21$) for the NBS 987 Sr standard. The total procedural blank was < 0.7 ng for Sr and ~0.1 ng for Rb. The Rb-Sr isotopic data (Table 8.3) were regressed using the ISOPLOT-Ex program of Ludwig (2001) and ages were calculated with 2σ errors. Rb and Sr concentrations were calculated offline by a double spike correction program.

Table 8.3 Rb-Sr isotopic data for carbonate–bearing dykes and pyrite residues of auriferous hydrothermal veins of Wynad

Sample number and location	Rb (µg/g)	Sr (µg/g)	$^{87}Rb/^{86}Sr^a$	$^{87}Sr/^{86}Sr \pm 2\sigma^b$	$^{87}Sr/^{86}Sr \pm 2\sigma^b$
Dykes					
W32E whole rock	8.9	446	0.057	0.70377 ± 21	–
W32E Fe-calcite	5.3	584	0.026	0.70301 ± 21	–
W32E musc 1	62	142	1.28	0.71099 ± 21	–
W32E musc 2	47	56	2.41	0.71838 ± 21	–
W2E whole rock	10	445	0.067	0.70324 ± 20	–
W2E Fe-calcite	6.4	533	0.0349	0.70300 ± 20	–
W2E musc	53	171	0.906	0.70824 ± 20	–
Pyrite residues					Pyrite fluids (only IC)
W21A py	3.3	7.4	1.30	0.70847 ± 20	–
W21C py	7.0	14	1.41	0.70858 ± 20	–
W21D py	2.3	7.8	0.859	0.70854 ± 20	–
W21E py	2.6	9.5	0.793	0.70878 ± 20	–
W22A py	3.5	16	0.679	0.70824 ± 20	0.70897 ± 20
W23A py	3.5	11	0.951	0.70826 ± 20	0.70894 ± 20
W23B py	3.2	11	0.806	0.70829 ± 20	0.70910 ± 20
W24A py	3.6	7.5	0.980	0.71175 ± 20	0.70886 ± 20
W26A py	4.2	15	0.813	0.70821 ± 20	0.70787 ± 20
W27B py	3.5	12	0.836	0.70823 ± 20	0.70841 ± 20
W28B py	2.5	9.5	0.757	0.70852 ± 20	0.70858 ± 20
W29A py	1.9	7.3	0.768	0.70864 ± 20	0.70992 ± 20

[a]Error of 1% on this ratio.
[b]Errors on least significant digits.

Mineral chemical analyses of selected phases were carried out on a Cameca SX100 electron probe microanalyzer, at the Institute Instrumentation Centre, IIT Roorkee, with an accelerating voltage of 15 kV and an electron beam current of 20 nA focused to <1 µ spot size. Counting times were 20 s on peak and 10 s on background; synthetic and natural standards were used for calibration of elements.
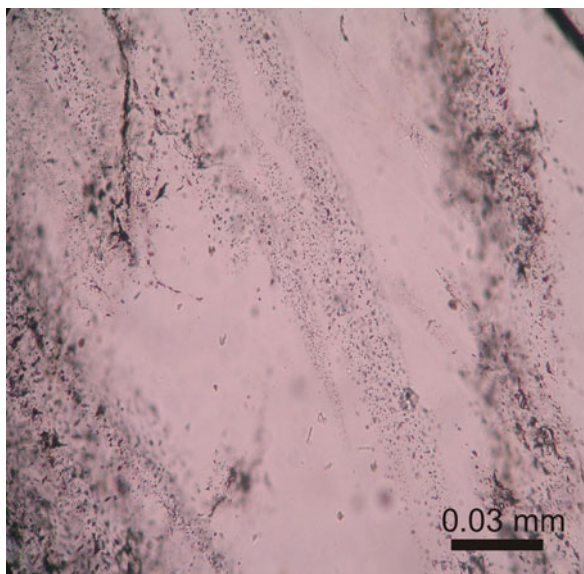
Results

Petrology

Gold-bearing quartz-pyrite veins, emplaced within faults and shears, represent late-stage hydrothermal veins originating from ~0.5 m thick, undeformed, pink quartz-carbonate dykes. Both hypidiomorphic and subvolcanic textures with carbonate and muscovite megacrysts set within a fine-grained groundmass are seen that have an assemblage comprising quartz + pyrite + phengite (muscovite-celadonite) + chlorite ($X_{Fe\ 0.79-0.84}$) + ankerite ($Ca_{0.47-0.58}$ [MgFe]$_{0.42-0.49}$) + ferran calcite ($Ca_{0.88-0.93}$

$Fe_{0.06–0.09}$) + albite ($Ab_{0–10}$) + gold + hematite + zircon. The sub-volcanic textured hydrothermal vein comprises quartz + pyrite ($Fe_{0.89–1.0}$ S_2) + muscovite + chlorite + ankerite ($Ca_{0.50–0.51}$ $[MgFe]_{0.46–0.49}$) + ferroan calcite ($Ca_{0.83–0}$ $Fe_{0.0–0.29}$) + albite + gold + hematite + zircon, whereas the primary hydrothermal veins which are being mined for gold have additional pyrrhotite and chalcopyrite ($Cu_{0.91–0.96}$ $Fe_{0.99–1.1}$ S_2). Secondary hydrothermal veins contain vugs and additional rutile.

Gold is exclusively hosted by pyrites in the auriferous quartz veins which are essentially arsenian (up to 1,700 ppm As). Binu Lal et al. (2003) have provided excellent photomicrographs of native gold occurring within pyrite. Powder X-ray diffraction patterns of these pyrites contain excess peaks indicating minor distortion of their structure. Compared to the ideal pyrite composition these pyrites have relatively low Fe ($Fe_{0.82–0.90}$ S_2 to $Fe_{0.89–1.0}$ S_2) and random spots analyzed by electron probe showed Au concentrations varying from 0.11 to 0.17 wt%. Brighter white patches within a background of grey visible in back scattered electron images have near-ideal pyrite compositions ($Fe_{0.92–1.0}$ S_2 to $Fe_{0.96–1.0}$ S_2). Grey pyrites show consistently low totals suggesting presence of volatiles but are particularly rich in Au and As. Energy dispersive spectroscopy revealed presence of C, O, Ca, Cl and K within grey pyrite suggesting inclusions of CO_2, calcite and KCl crystals. Similar densely populated gas-rich fluid inclusions are also seen in quartz from the auriferous hydrothermal veins (Fig. 8.3).

Fig. 8.3 CO_2 and H_2O rich gas-rich fluid inclusions in quartz from auriferous hydrothermal veins of Wynad

Geochemistry of Fluids

As the pyrites were considered to be diagnostic of gold mineralization (being transported as sulfide complexes and precipitated at low temperatures along with pyrite, Binu Lal et al., 2003), we extracted the water-soluble component of the

fluid inclusions by crushing selected pyrite samples dipped in MilliQ water. The results of such analyses are shown in Table 8.1 and the chondrite- (after Sun and McDonough, 1989) and primitive upper mantle (PUM)-(after McDonough et al., 1991) normalized patterns are shown in Figs. 8.4a and b. The most diagnostic
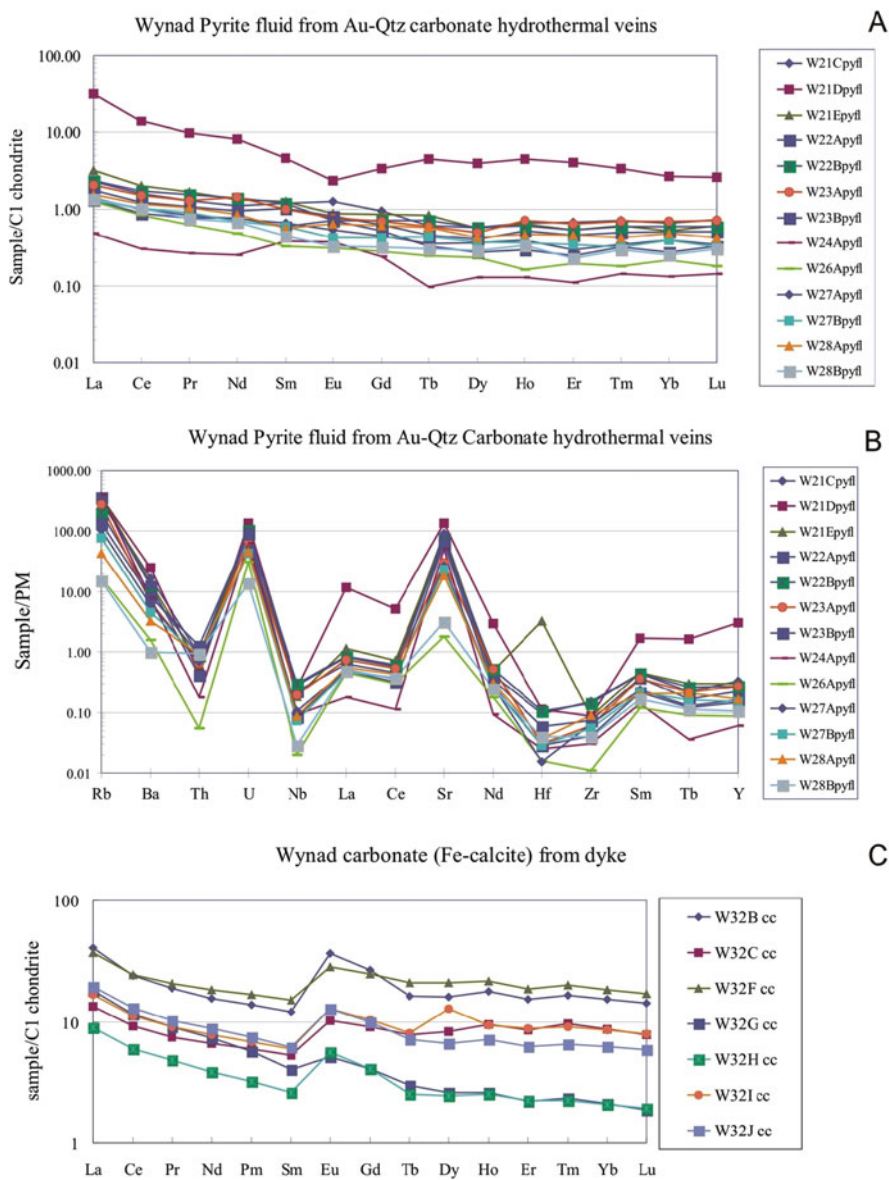

Fig. 8.4 (**a**) Chondrite (C1 of Sun and McDonough, 1989) normalized REE plot of fluid extracted from the pyrite. (**b**) Primitive mantle normalized (McDonough et al., 1991) spidergram of fluid extracted from the pyrite and ferroan calcite (**c**)

feature of these fluids is that they are in general depleted in trace elements with respect to the PUM except for Rb, Ba, Sr and U and have a near flat chondrite normalized REE pattern, suggesting juvenile source(s) to these fluids. Ferroan calcite from the auriferous hydrothermal veins were also analyzed for their trace and REE contents (Table 8.2) and are shown on Fig. 8.4c which show subequal LREE/HREE and positive Eu anomalies, characteristic of derivation from plagioclase breakdown.

Sr Isotope Geochemistry of the Dykes

Rb-Sr isotopic analyses were conducted from a quartz-carbonate dyke (W32) using the phases muscovite (fine fraction), muscovite (coarse flakes), whitish calcite, and whole rock fraction and a typical hydrothermal vein that cross-cuts the tonalitic gneiss (W2E) from which ankerite and muscovite along with its whole rock were analyzed. Similarly, Sr isotopic composition of pyrite fluids, separated from twelve hydrothermal auriferous veins and Rb-Sr isotopic analyses of the pyrite residues, were conducted; all isotopic analyses are given in Table 8.3. Isotopic ratios from the dyke, W32, yielded an Rb-Sr age of 443 ± 18 (2σ), MSWD = 1.6, with $Sr_i = 0.7031 \pm 0.0003$ (2σ) whereas the auriferous hydrothermal vein, W2E, yielded an age of 420 ± 35 (2σ), MSWD = 0.038, with $Sr_i = 0.7028 \pm 0.0003$ (2σ). Regressing all seven data from the dyke and vein yielded an age of 446 ± 26 (2σ), MSWD = 2 with $Sr_i = 0.7029 \pm 0.0004$ (2σ) (Fig. 8.5). The age-corrected (at 450 Ma) Sr
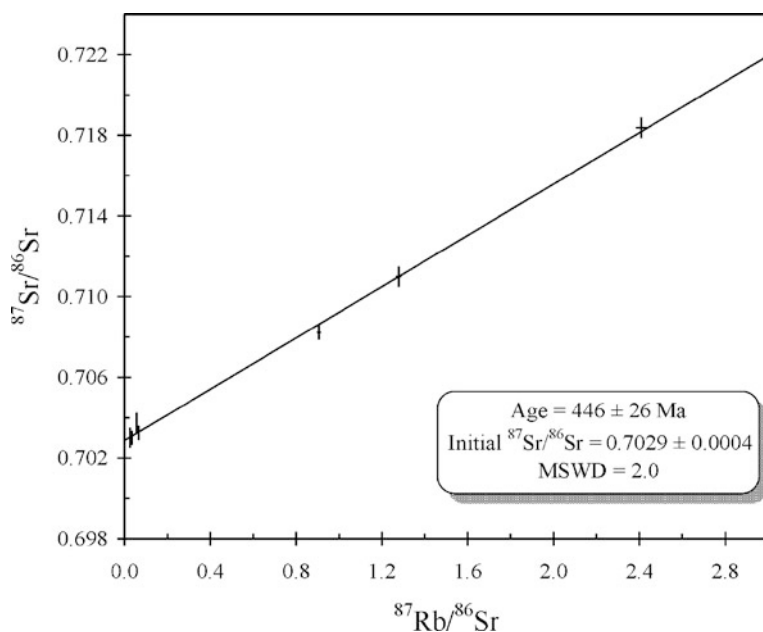

Fig. 8.5 Rb-Sr isochron diagram regressing phases from both quartz-carbonate dyke (sample W32) and auriferous hydrothermal vein (sample W2E) of SW Wynad

initial ratios of the pyrite residues also are tightly constrained to between 0.70216 and 0.70389; regressing the pyrite residues along with the seven-points from the quartz-carbonate dykes yields an isochron age of 445 ± 35 (2σ), MSWD = 7.6 with an $Sr_i = 0.7031 \pm 0.0005$.

Discussion

Generally gold mineralization in southern India is ascribed to magmatic intrusives, hydrothermal exhalatives, metamorphic outgassing in greenstone belts or to a combination of all of them. Our observations indicate that the auriferous hydrothermal veins of the Wynad Gold Field, one of the very few occurrences in the Southern Granulite Terrain, are undeformed rocks intrusive into polydeformed high-grade metamorphic rocks. Rather than by any crustal scale shear zone, their emplacement was controlled by late-stage brittle fracture-fault systems that are clearly younger than any tectonothermal event. This makes these dykes potentially amenable to geochemical study.

Mantle-derived (cryptic) intrusions (alkali basalt, syenite and carbonatite) of Neoproterozoic age (~800 Ma) acted as source(s) to the extensive carbonate influx in the Attur shear zone as deciphered by Wickham et al. (1994). Although regional carbonate alteration zone features of the Attur area have petrologic similarities with those observed in the Wynad area and both these occurrences lie proximal to the E-W trending Moyar-Attur crustal-scale shear zone, these alteration zones do not seem to be coeval. From the Attur area, whole rock, muscovite and carbonate isochrons yield dates of 439 and 494 Ma with high initial $^{87}Sr/^{86}Sr$ ratios of 0.7095 and 0.7074, respectively. Although these dates are similar to those obtained in this study, from the Wynad quartz-carbonate dykes (~450 Ma), the initial $^{87}Sr/^{86}Sr$ ratios of the Wynad samples are very low (0.7030) and distinctly resemble mantle ratios in contrast to the higher initial ratios of the Attur samples as reported by Wickham et al. (1994), who interpret these ages as that of retrogression and hydration postdating granulite-facies metamorphism in the Southern Granulite Terrain.

As discussed by Barker (1989), if the carbon of a carbonatite is juvenile being derived from identifiable or suspected magmas, then carbonate-rich rocks, can be considered as having been derived from cryptic carbonatite intrusions. Because no relative LREE enrichment was observed in our pyrite fluid analyses (Fig. 8.3a) and in the absence of any reported carbonatite intrusions around Wynad, we discount the link to carbonatite for gold mineralization in these quartz-carbonate veins. Furthermore, the carbon of the carbonate fraction from auriferous hydrothermal veins in the Wynad area was shown, using stable isotope ratios of carbonate inclusions in quartz, by Santosh et al. (1995) to have been derived from the mantle. This is also clearly supported by our low initial Sr isotopic ratios from the quartz-carbonate dykes. As carbonate influx occurred definitely postdating the ~500–550 Ma Pan-African tectonothermal event (deformation ceased by ~490 Ma, e.g. Meiβner et al., 2002) in the Wynad area, this would then constrain the age of the mantle/lower crust-derived fluid influx to be late Pan-African. In addition, we have shown that

the fluids trapped within the pyrites (ubiquitously associated with gold) possess a near-flat chondrite normalized REE pattern, again strongly suggesting that the fluids were directly derived from the mantle/lower crust, and not from any carbonatite or lamprophyre melt.

The predominance of quartz and carbonate with a low sulfide-content in the auriferous veins, emplaced along brittle-ductile fractures, and the association of chlorite-carbonate-sericite alteration of the host rock suggest the orogenic nature of the gold mineralization (Goldfarb et al., 2001). Further, the age of the mineralization (~450 Ma) links its genesis to the structural and thermal events of the Pan-African orogenic cycle in the Southern Granulite Terrain. Thus the distinct mantle/lower crust signatures of these dykes further corroborates that the gold mineralization is of orogenic type and occurred due to mantle/lower crust-derived CO_2–rich fluids (carbonate flux).

Conclusions

1. In the Wynad Gold Field of the Southern Granulite Terrain, auriferous quartz-pyrite veins, emplaced within faults and shears, represent late-stage hydrothermal veins originating from ~0.5 m thick, undeformed, pink quartz-carbonate dykes. These quartz-carbonate dykes have been dated at ~450 Ma, with very low initial $^{87}S/^{86}Sr$ isotopic ratios (0.7029) and have nearly flat chondrite normalized REE values.
2. In conjunction with earlier isotopic analyses of carbon from carbonates of auriferous veins that indicates its mantle/lower crustal derivation, the Sr isotopic data and nearly flat chondrite normalized REE pattern, strongly suggest a mantle-derived carbonate fluid that transported the gold. The gold mineralization is orogenic type related to post-Pan-African orogeny processes.

References

Banks DA, Wayne D, Miller M, Scrivner R (1992) Composition and origin of ore-fluids in the SW-England orefield. Pan American Conference on Research in Fluid Inclusions (PACROFI) 4: 12

Barker DS (1989) Field relations of carbonatites. In: Bell K (ed) Carbonatites-Genesis and Evolution. Unwin Hyman, London: 38–69

Barnicoat AC, Fare RJ, Groves DI, McNaughton NJ (1991) Synmetamorphic lode-gold deposits in high-grade settings. Geology 19: 921–924

Binu Lal SS, Sawaki T, Wada H, Santosh M (2003) Ore fluids associated with the Wynad gold mineralization, southern India: Evidence from fluid inclusion microthermometry and gas analysis. J Asian Earth Sci 22: 171–187

Bottrell SH, Yardley BWD, Buckley F (1988) A modified crush-leach method for the analysis of fluid inclusion electrolytes. Bull Mineral 111: 279–290

Channer DM, De R, Bray CJ, Spooner ETC (1999) Integrated cation-anion/volatile fluid inclusion analysis by gas and ion chromatography: Methodoloy and examples. Chem Geol 154: 59–82

Christensen JN, Halliday AN, Leigh KE, Randell RN, Kesler SE (1995) Direct dating of sulfides by Rb-Sr: A critical test using the Polaris Mississippi Valley-type Zn-Pb deposit. Geochim et Cosmochim Acta 59(24): 5191–5197

Ghosh JG, DeWit M, Zartman RE (2004) Age and tectonic evolution of Neoproterozoic ductile shear zones in the Southern Granulite Terrain of India, with implications for Gondwana studies. Tectonics 23 doi: 10.1029/2002TC001444

Goldfarb RJ, Groves DI, Gardoll D (2001) Orogenic gold and geologic time: A global synthesis. Ore Geol Rev 18: 1–75

Groves DI, Barley ME, Ho SE (1989) Nature, genesis, and tectonic setting of mesothermal gold mineralization in the Yilgarn Block, Western Austarlia. In: Keays RR, Ramsay WRH, Groves DI (eds) The Geology of Gold Deposits. Econ Geol Monogr 6: 71–85

Groves DI, Goldfarb RJ, Robert F, Craig JRH (2003) Gold deposits in metamorphic belts: Overview of current understyanding, outstanding problems, future research and exploration significance. Econ Geol 98: 1–29

Kerrich R (1990) Carbon-isotope systematics of Archean Au-Ag vein deposits in the Superior Province. Can J Earth Sci 27: 40–56

Kerrich R, Fryer BJ, King RW, Willmore LM, van Hees E (1987) Crustal outgassing and LILE enrichment in major lithospheric structures, Archean Abitibi greenstone belt: Evidence on the source reservoir from strontium and carbon isotope tracers. Contrib Mineral Petrol 97: 156–168

Ludwig KR (2001) User Manual for Isoplot/Ex version 2.47. A geochronological tool kit for Microsoft Excel, Berkeley Geochronology Center Special Publication 2: 19

Malathi MN, Srikantappa C (2005) Composition and evolution of fluids and timing of gold mineralization in the Malappuram-Gudalur and Bhavani shear zone, Nilambur, Kerala. J Geol Soc India 65: 689–702

McDonough WF, Sun S-s, Ringwood AE, Jagoutz E, Hofmann AW (1991) K, Rb, and Cs in the earth and moon and the evolution of the earth's mantle. Geochim Cosmochim Acta 56: 1001–1012

Meiβner B, Deters P, Srikantappa C, Kohler H (2002) Geochronological evolution of the Moyar, Bhavani and Palghat shear zones of southern India: Implications for east Gondwana correlations. Precamb Res 114: 149–175

Nair RS, Suresh CM (1994) Gold mineralization in Kappil prospect, Malappuram district, Kerala. J Geol Soc Ind 43: 573–583

Ravikant V (2010) Palaeoproterozoic (~1.9 Ga) extension and rifting along the eastern margin of the Eastern Dharwar Craton, SE India: New Sm-Nd isochron age constraints from anorogenic mafic magmatism in the Neoarchean Nellore greenstone belt. J Asian Earth Sci 37: 67–81

Santosh M, Nadeau S, Javoy M (1995) Stable isotope evidence for the involvement of mantle-derived fluids in Wynad gold mineralization, South India. J Geol 103: 718–728

Santosh M, Sajeev K (2006) Anticlockwise evolution of ultrahigh temperature granulites within continental collisional zones in southern India. Lithos 92: 447–464

Sun S-s, McDonough WF (1989) Chemical and isotopic systematics of oceanic basalts: Implications for mantle composition and processes. In Saunders AD, Norry MJ (eds) Magmatism in ocean basins. Geol Soc Lond Spl Publ No 42: 313–345

Wickham SM, Janardhan AS, Stern RJ (1994) Regional alteration of the crust by mantle-derived magmatic fluids, Tamil Nadu, South India. J Geol 102(4): 379–398